Bioelectrochemistry 141 (2021) 107838

Contents lists available at ScienceDirect

Bioelectrochemistry

journal homepage: www.elsevier.com/locate/bioelechem

A feasible electrochemical biosensor for determination of glucose based on Prussian blue – Enzyme aggregates cascade catalytic system

Long Yan, Kunpeng Miao, Pengcheng Ma, Xiaoyan Ma *, Ran Bi, Fang Chen

The Key Laboratory of Space Applied Physics and Chemistry, Ministry of Education, Northwestern Polytechnical University, Xi'an 710129, PR China

ARTICLE INFO

Article history:
Received 31 January 2021
Received in revised form 12 April 2021
Accepted 3 May 2021
Available online 06 May 2021

Keywords:
Prussian blue
Hydrogen peroxide
Cross-linking enzyme aggregates
Glucose biosensor

ABSTRACT

The coral-like gold micro/nanostructures were formed onto carbon cloth followed by a Prussian blue (PB) electrochemical deposition to construct a highly sensitive H_2O_2 biosensor. The SEM image of PB/Au/CC showed the coral-like gold morphology, and EDS and XPS tests also further confirmed the successful loading of Au and PB. The electrochemical tests of PB/Au/CC displayed the electrode possessed excellent performance in sensing H_2O_2, which was quantified in the linear range from 0.002 to 13.97 mM at an applied potential of −0.05 V, with a sensitivity of 454.97 μA mM^{-1} cm^{-2} and a detection limit of 0.5 μM (S/N = 3). And then a convenient sensing platform was established via the cross-linking enzyme aggregates method, using PB as the mediator to realize the construction of glucose BIOSENSOR GOx_{EA}@PB/Au/CC. The biosensor responded to glucose in the sensitivity of 70.76 μA mM^{-1} cm^{-2} within the linear range from 0.05 to 3.15 mM with a detection limit of 10 μM. The sensitivity was much higher than the electrode constructed by the cross-linking enzyme method (GOx@PB/Au/CC), and it was also highly selective, reproducible, and stable. Besides, the proposed biosensor was successfully applied to the glucose determination in real human serum samples, which proved its practicability.

1. Introduction

Data released in 2019 by the International Diabetes Federation indicates that 460 million diabetes worldwide nowadays is projected to rise to 580 million in 2030 and 700 million by 2045 [1]. With the continuous rise in diabetics, blood glucose monitoring has received much attention as it is the most effective way to prevent, diagnose, and intervene in the development of diabetes [2]. Established methods for the detection of glucose levels can be roughly divided into three types [3]. The first is to detect variations in color based on chemical reactions [4], the second is to observe the refractive index changes by employing optical techniques [5,6], and the last approach is to calculate the electrochemical characteristics. Among them, electrochemical enzymatic biosensors have drawn much attention due to the outstanding advantages, including a low limit of detection (LOD), high sensitivity, and good selectivity [7,8].

Although glucose self-monitoring has been widely accepted and provides a significant improvement in the quality of life for diabetic patients, it is limited by the number of routine examinations and discomfort caused by the invasive method. Thus, there is a considerable demand for optimized sensing technologies for implantable continuous glucose monitoring [9,10]. GOx is one of the routine biocatalysts used for glucose oxidation in organisms, but in the presence of oxygen, it would react with glucose to generate toxic by-product H_2O_2 [11,12] and may deteriorate the long-term stability of biosensors [13]. The multi-enzyme electrode has been constructed through co-immobilization of GOx and peroxidase or other enzymes for addressing this issue [14,15]. Nevertheless, the enzymes, being inherently fragile, obviously cannot keep the long-term stability [16]. Besides, continuous glucose monitoring for integrated biosensors needs the development of reagentless biosensors independent of free diffusing redox mediators [17]. Prussian blue (PB), a kind of mixed-valence compound formed by the coordination of iron ions and CN bridges, has been described as an "artificial peroxidase" that exhibits an excellent peroxidase-like catalytic performance towards H_2O_2 [18]. Moreover, the reported catalytic constant of PB is three orders of magnitude higher than that of natural peroxidase [19,20]. In previous studies, they have been extensively applied to the sensing of hydrogen peroxide at a very low applied potential, enabling the incorporation of oxidase enzymes to sense the corresponding substrate while minimizing the influence of other electrochemical interferents. More importantly, as an inorganic conductive film, PB can be easily attached to the electrode and replace the free

* Corresponding author.
E-mail address: m_xiao_yana@nwpu.edu.cn (X. Ma).

https://doi.org/10.1016/j.bioelechem.2021.107838
1567-5394/

electron transfer mediator in the solution to directly generate electrochemical signals, thereby realizing the fabrication of reagentless electrochemical biosensors. Zhang et al. [21] used this approach to detect the current corresponding to the reduction of H_2O_2 occurring at the nitrogen-doped graphite foam electrode modified with PB and GOx and thus indirectly to determine the glucose concentration. Ramanavicius et al. [22] designed three types of electrodes based on polypyrrole, GOx, and PB to realize amperometric glucose biosensors.

Recently, the cross-linking enzyme aggregates (CLEAs) has shown great potential as an attractive enzyme immobilization method with its exquisite simplicity and robustness [23]. The preparation of CLEAs involves aggregation or precipitation of the enzyme (that may be pure or not) without perturbation of their tertiary structure and chemical cross-linking of the resulting physical enzyme aggregates. Precipitation/aggregation is usually formed by introducing salts, organic solvents, or non-ionic polymers to the enzyme solution. And the resulting enzyme aggregates are then cross-linked by the use of bifunctional agents [24]. In this method, the cross-linked enzyme aggregates can be attached to the nanomaterials' surface in the form of an enzyme aggregates coating, and the unbound or slightly bound cross-linked enzyme aggregates can be excessively washed away [25]. Compared with the common cross-linking enzymes (CLEs), it is more effective since it could significantly maintain the enzyme activity and enzyme loading [26].

In the present study, we used a coral-like gold modified carbon cloth flexible electrode as the substrate and decorated it with PB to construct the H_2O_2 sensor that exhibits high electrochemical sensing capabilities. Inspired by the fact that H_2O_2 is the by-product of glucose enzymolysis, a convenient reagent-less glucose sensing platform was established via combining cross-linking enzyme aggregates, based on PB's redox property providing self-mediation. To our best knowledge, there is no publication on glucose biosensors employing an electrode combined with enzyme aggregates and PB. Only with one more step of enzyme aggregation, the glucose biosensor can achieve a substantial improvement in the sensing performance.

2. Materials and methods

2.1 . Chemicals and equipment

Carbon cloth (hydrophilic W0S1009) was received from Taiwan CeTech Co., Ltd.. Gold chloride trihydrate ($HAuCl_4{\cdot}3H_2O$, Aladdin), potassium ferricyanide ($K_3[Fe(CN)_6]$, Aladdin), iron chloride hexahydrate ($FeCl_3{\cdot}6H_2O$, Aladdin), potassium chloride (KCl, Aladdin), glucose oxidase (GOx) from Aspergillus niger (100 U mg^{-1}, Aladdin), β-d-Glucose ($C_6H_{12}O_6$, Aladdin), ammonium sulfate ($(NH_4)_2SO_4$, Aladdin), glutaraldehyde ($C_5H_8O_2$, Aladdin), uric acid ($C_5H_4N_4O_3$, Aladdin), ascorbic acid ($C_6H_8O_6$, Aladdin) and dopamine ($C_8H_{11}NO_2$, Aladdin) were analytical reagent and used as received. Other reagents were all purchased from Tianjin Damao Co., Ltd.. Deionized (DI) water was used throughout all the experiments. The human serum samples are provided by the first author and this study is approved by the Ethics Committee of Northwestern Polytechnical University.

The surface morphology and structure of the obtained electrode were characterized by the Field Emission Scanning Electron Microscope (FE-SEM, FEI Verios G4, America). And the elemental analysis was performed by the energy dispersive spectrometer equipped in FEI Verios G4. X-ray photoelectron spectroscopy (XPS, Kratos AXIS Ultra DLD, energy spectrum instrument with Al Kα source) analysis was tested to examine the chemical composition and redox state of PB/Au/CC. Electrochemical measurements were done by the CHI660E electrochemical workstation (Shanghai CH Instruments Co. Ltd.) with a three-electrode setup at room temperature.

2.2. Fabrication of the PB/Au/CC electrode

A piece of carbon cloth (CC) was ultrasonically cleaned with ethanol, acetone, and ultrapure water in sequence, and then dried at 60 ℃[27]. After drying, the cleaned CC was employed as the substrate material for Au electrodeposition. A constant potential (as high as − 4 V) was applied in a stationary 0.5 M H_2SO_4 + 0.005 M $HAuCl_4$ solution for Au electrodeposition (designated as Au/CC).

The Au/CC electrode was then immersed into the growth solution, and a constant applied potential of 0.4 V was performed within 150 s. The growth solution was composed of 3.0 mM $K_3[Fe(CN)_6]$, 3.0 mM $FeCl_3$, dissolved in 0.1 M KCl + 0.01 M HCl [28]. After electrodeposition, the PB layer was activated by CV within the potential range of − 0.05 V to 0.35 V until a stable CV curve appeared. Then the electrode was dried at 100 °C for 1 h, and PB modified Au/CC (PB/ Au/CC) was stored at room temperature.

2.3. Fabrication of the GOx_{EA}@PB/Au/CC electrode

The PB/Au/CC electrode was incubated into 10 mg mL^{-1} of GOx solution for 2 h. Then ammonium sulfate solution was added into the GOx solution to precipitate the free GOx out to form the enzyme aggregates (GOx_{EA}) in the vicinity of the PB/Au/CC electrode. After 30 mins, glutaraldehyde (GA) was added into the solution to crosslink the GOx_{EA} and incubated at 4 °C overnight. Finally, GOx_{EA}@PB/Au/CC was excessively washed with PBS.

2.4 . Electrochemical detection of hydrogen peroxide and glucose

The Ag/AgCl (saturated KCl), Pt wire, and test sample were employed as reference electrode, counter electrode, and working electrode, respectively. For the amperometry i-t tests, − 0.05 V was applied to the working electrode in 0.1 M PBS (pH 6.0) containing 0.1 M KCl.

3. Results and discussion

The synthetic process of electrode is summarized schematically in Scheme 1 (see Experimental section for details).

3.1. Morphology and constituent characterization of electrodes

The morphologies of the obtained electrodes were investigated by FE-SEM. As is shown in Fig. 1A, the original CC is woven by carbon fibers, tightly packed together, and exhibits an entirely smooth surface. Such well- intertwined three-dimensional structures can provide a conductive network and large specific surface area. After Au electrodeposition, the free-standing coral-like gold coatings are formed on the carbon cloth substrate with a 3D skeleton as revealed by the SEM image (Fig. 1B). The reason for the formation of this morphology has been explained in our previous work. The coral-shaped structure occurs mainly because we have chosen a sufficiently negative potential at which H + can be reduced when the electrodeposition of gold takes place. As hydrogen evolution occurs, a turbulent layer is formed over the electrode surface which would disturb Au deposition and the formation of new nucleation sites. Once the formation of new nucleation sites is hindered, any growth from the formed nucleation sites would develop as branches and finally form gold films with coral-shaped morphology [29]. The micrograph for the CC shows a very plain surface, while the Au/CC shows a very rough surface due to the electrode-

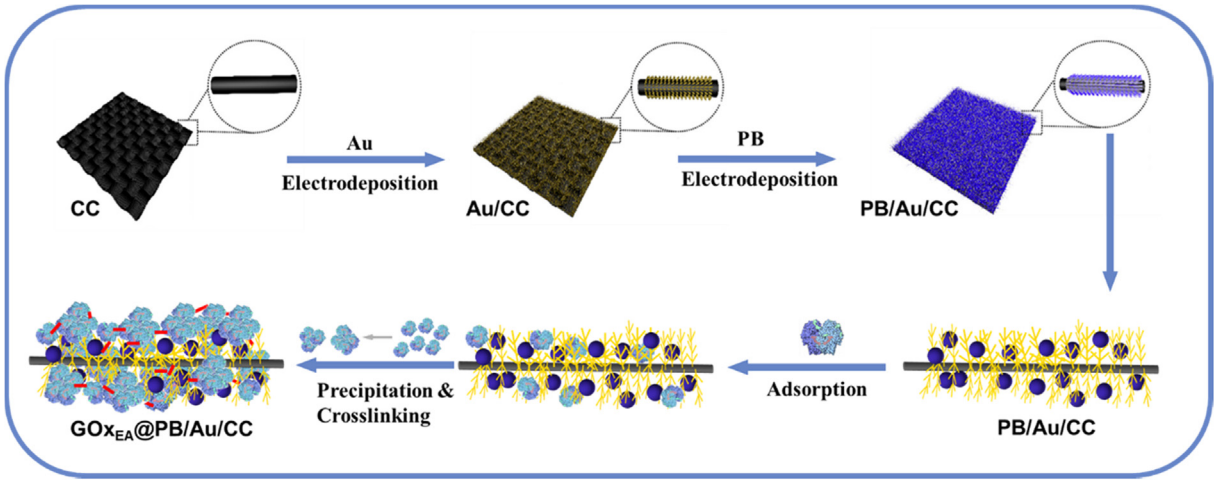

Scheme 1. The schematic diagram of the formation process of the GOx$_{EA}$@PB/Au/CC electrode.

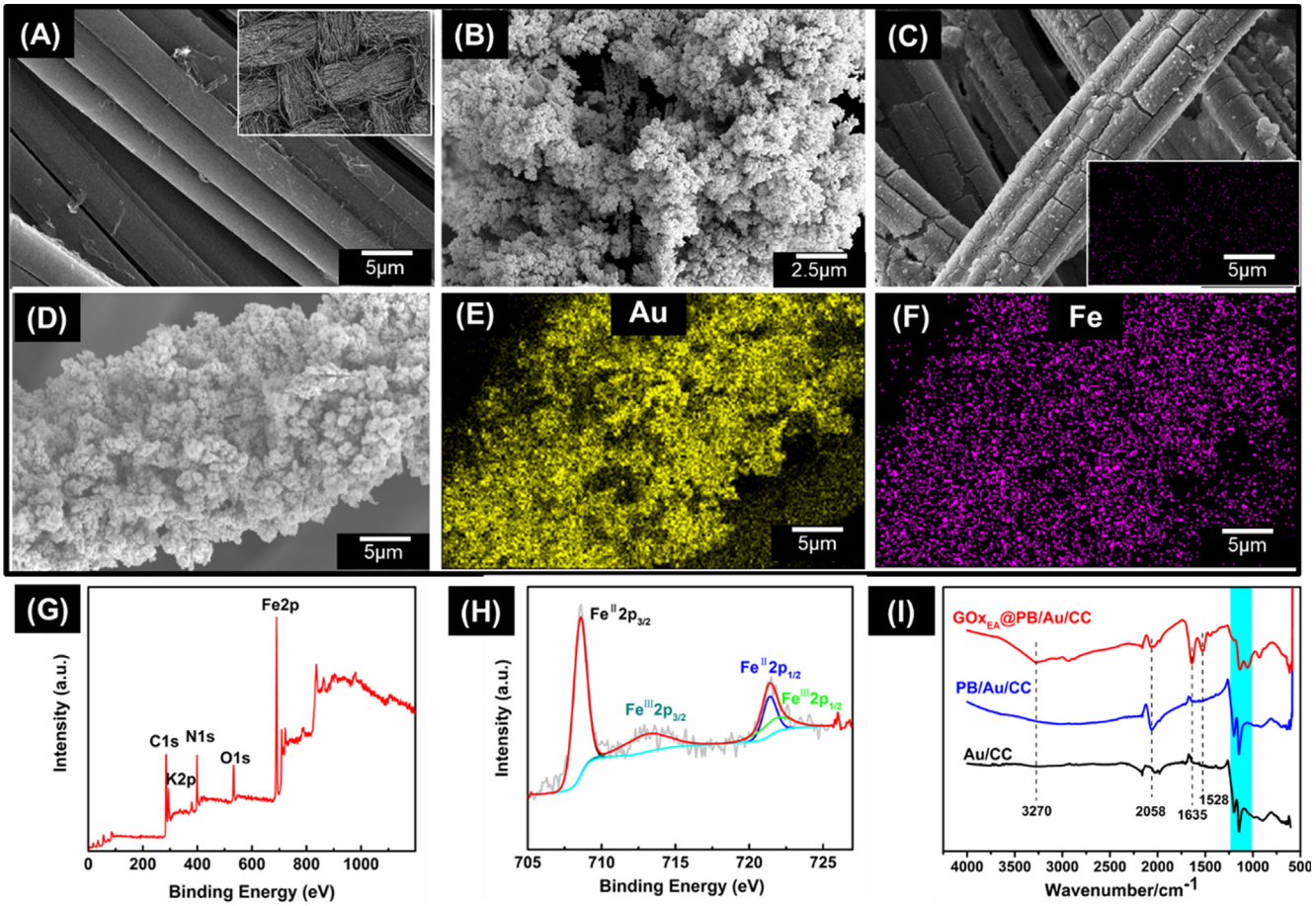

Fig. 1. SEM micrographs of (A) CC, (B) Au/CC, (C) PB/CC, (D) PB/Au/CC, and EDS mapping results of (E) Au, (F) Fe on the PB/Au/CC. (G) XPS plot and (H) Fe 2p spectra of PB/Au/CC. (I) FTIR spectra of Au/CC, PB/Au/CC, and GOx$_{EA}$@ PB/Au/CC.

position of Au. Compared with the flat interface of traditional electrodes, the abundant positions for loading target catalysts can be successfully obtained in the stereoscopic space of Au/CC [30].

After PB was deposited onto Au/CC, the original morphology was not destroyed (Fig. 1D), and at the same time, we used the energy-dispersive X-ray spectroscopy (EDS) elemental mapping analysis to explore the elemental composition, to confirm the intercalation of PB into the coral-like Au coatings and the distribution of PB on carbon cloth (Fig. 1F). Furthermore, X-ray photoelectron spectroscopy (XPS) was performed on PB/Au/CC to analyze the elemental composition and redox state of PB. As shown in Fig. 1G, the peaks of C (1s), N (1s), Fe (2p), and K (2p) all appear in the spectrum, which indicates the elemental composition of PB. The high-resolution spectrum of Fe 2p in Fig. 1H is further analyzed. The fitted curve mainly consists of two clusters of peaks located at 708.6 and 721.4 eV, corresponding to Fe^{II} 2p$_{3/2}$ and Fe^{II} 2p$_{1/2}$ in the [Fe

$(CN)_6]^{4-}$group. Meanwhile, the satellite peaks at 713.0 and 722.7 eV can be attributed to Fe^{III} $2p_{3/2}$ and Fe^{III} $2p_{1/2}$ which coordinating with N in the PB crystal structure. XPS spectrum is consistent with the previous report [31].

The as-prepared Au/CC, PB/Au/CC, and GOx_{EA}@ PB/Au/CC were investigated by FTIR spectroscopy. Peaks at 1000–1300 cm^{-1} are ascribed to C–O single bonds in the CC. Most carbons contain hydrogen, and band of C–H stretch and wagging vibrations are observed [32]. The FTIR spectrum of PB/Au/CC comprised a characteristic band at 2058 cm^{-1}, which corresponds to the C≡N bond stretching [33,34]. The peak with a wavenumber of 1635 cm^{-1}, attributed to the amide I bond (1700–1600 cm^{-1}), is caused by the stretching vibration of C═O at the junction of the peptide in the backbone of the GOx. The amide II bond with a wavenumber of 1528 cm^{-1} in the FTIR spectra is originated from the bending of N-H and the stretching vibration of C—N [35].

3.2. Electrochemical reactivity of electrodes

To further prove the effectiveness of gold deposition on the modified electrode, we performed chronocoulometry and cyclic voltammetry (CV) measurements on CC and Au/CC by using the $[Fe(CN)_6]^{3-/4-}$ redox probe. In the same electrochemistry system, the slope of the Q-$t^{1/2}$line is proportional to the relative apparent electrode area (A)[36]. From the slope of the Q-$t^{1/2}$ line, the order of the A values is Au/CC > CC, which means that the relative apparent area of the CC electrode increases after the coral-like gold coating is electrodeposited. Fig. 2B shows the quasi-reversible electrochemical behavior of the redox probe on the CC and Au/CC surface, and the redox peak current of CC/Au is found to be much more evident as compared to that of CC. This may be due to the electrodeposition of Au on the CC surface, leading to the improvement of the effective area and the electron transport kinetics of the electrode.

To electrochemically characterize the GOx_{EA}@PB/Au/CC construction, CVs of different preparation steps were performed in mediator-free PBS (pH 6.0) containing 0.1 M KCl. As Fig. 2C shows, it is found that there is no evident redox peak on CC and Au/CC for lack of an electrochemical redox mediator. After the PB layer was electrodeposited on the CC and Au/CC electrode, a pair of well-defined waves assigned to the PB redox reactions at the electrode can be observed. Moreover, the redox peak of PB/Au/CC is more obvious than that of PB/CC, which indicates that an electroactive surface with higher electrochemical activity is realized by the electrodeposition of PB on the Au/CC. When GOx was immobilized on the PB/Au/CC electrode, the peak current of GOx_{EA}@PB/Au/CC decrease significantly o owing to the non-conductive nature of enzymes, thereby inhibiting the electron transfer of PB. The obtained results also proved that GOx has been attached successfully to the PB/Au/CC electrode (GOx_{EA}@PB/Au/CC).

It is generally to study the electron transfer properties of different electrodes by employing electrochemical impedance spectroscopy (EIS). The diameter of the semicircular arc at high frequencies is attributed to the electron transfer resistance (Ret), which reflects the electron transfer kinetics of the redox reaction on the electrode surface, while at lower frequencies, the linear part is due to Warburg diffusion. As shown in Fig. 2D, the Ret of modified electrodes is in the sequence of GOx_{EA}@PB/Au/CC (48.4 Ω) > CC (7.5 Ω) > PB/CC (4.4 Ω) > Au/CC (3.2 Ω) > PB/Au/CC (0.8 Ω), and the Ret of PB/CC is lower than that of the CC, which can be explained by the PB layer promoting electron transfer from the redox probe to the electrode surface. Obviously, PB/Au/CC shows a relatively low Ret value, which indicates that the electrode is suitable for use as a substrate for immobilizing GOx. Moreover, the electrode of GOx_{EA}@PB/Au/CC possesses the largest Ret, reflecting that GOx has been attached to the electrode surface and the immobilized amount is large.

In general, the electrochemical kinetics could be derived from the dependence of peak current values on changing scanning rates from CV curves. As the detection mechanism of H_2O_2 relies primarily on PB, the effect of changing scan rates on the redox peak current and peak separation of PB/Au/CC has been studied. Fig. 2E exhibits the CV curves at different scan rates from 10 to 200 mV s^{-1} in 0.1 M PBS (pH 6.0). The increase in scan rate results in the increase in current and separation between the reduction and oxidation peaks. And the CV curve can still retain the original shape even under a relatively high scan rate of 200 mV s^{-1}, reflecting the high conductivity of the electrode. This process, as can be observed in Fig. 2F, reflects a linear dependence with the scan rate, indicating fast electron transfer kinetics at PB/Au/CC and a typical surface-controlled process.

3.3. H_2O_2 determination by PB/Au/CC

The electrochemical reaction of the H_2O_2 on the PB/Au/CC was demonstrated by using the CV and amperometric measurements.

In Fig. 3A shows the CV curves of the PB/Au/CC electrode in 0.1 M PBS (pH 6.0) containing 0.1 M KCl with or without adding H_2O_2. According to the result, in the absence of H_2O_2, a pair of well-defined redox waves with formal potential at 0.14 V can be observed (curve a), which can be attributed to the PB/Prussian white (PW) redox transition shown in the Eq. (1). When adding H_2O_2 to the solution, an obvious increase of cathodic peak current appears with a decrease in the anodic peak current (curve b) due to the PB catalytic reduction of H_2O_2. The reaction can be described by the well-known mechanism shown in Eq. (2).

$$\underset{PB}{Fe_4[Fe(CN)_6]_3} + 4K^+ + 4e^- \rightleftharpoons \underset{PW}{K_4Fe_4[Fe(CN)_6]_3} \quad (1)$$

$$\underset{PW}{K_4Fe_4[Fe(CN)_6]_3} + 2H_2O_2 \rightleftharpoons \underset{PB}{Fe_4[Fe(CN)_6]_3} + 4K^+ + 4OH^- \quad (2)$$

In Fig. 3B and 3D show the amperometric i-t response at the PB/CC and PB/Au/CC electrode under the applied potential of −0.05 V. The calibration plot of the steady-state current on PB/CC (Fig. 3C) and PB/Au/CC (Fig. 3E) along with H_2O_2 concentration demonstrates that the linear response range of the biosensor can reach 3.27 and 13.97 mM, respectively. The regression equation of the linear part is Ipc (μA) = 139.1C (mM) + 37.46 and Ipc (μA) = 454.97C (mM) + 89.20 with R^2 of 0.999, respectively. The sensitivity of PB/CC is 139.1 μA $mM^{-1}cm^{-2}$ with LOD of 2 μM (S/N = 3). And the sensitivity of PB/Au/CC is 454.97 μA $mM^{-1}cm^{-2}$ and LOD is 0.5 μM. By comparing the sensing performance of the above two electrodes, it can be clearly seen that the electrode PB/Au/CC we constructed has a higher H_2O_2 electrocatalytic reduction ability. This indicates that the electrodeposition of coral-like gold micro/nanostructures is essential for the construction of a high-performance H_2O_2 biosensor.

Table 1 displays the sensing performance of different electrodes, including sensitivity, LOD and linear range. It can be seen from Table 1 that our H_2O_2 biosensor possesses absolute advantages, especially in such a convenient and quick fabrication way, which relies in the unique design of our electrode. In other words, the porous three-dimensional interconnection structure of coral-like gold-modified CC can easily load a large amount of PB and create a lower mass transfer resistance. Moreover, the gold coating can accelerate the transfer of electrons to the electrode surface.

To investigate the stability of PB, the PB/Au/CC electrode was tested by CV in 0.1 M PBS containing 0.1 M KCl after scanning for

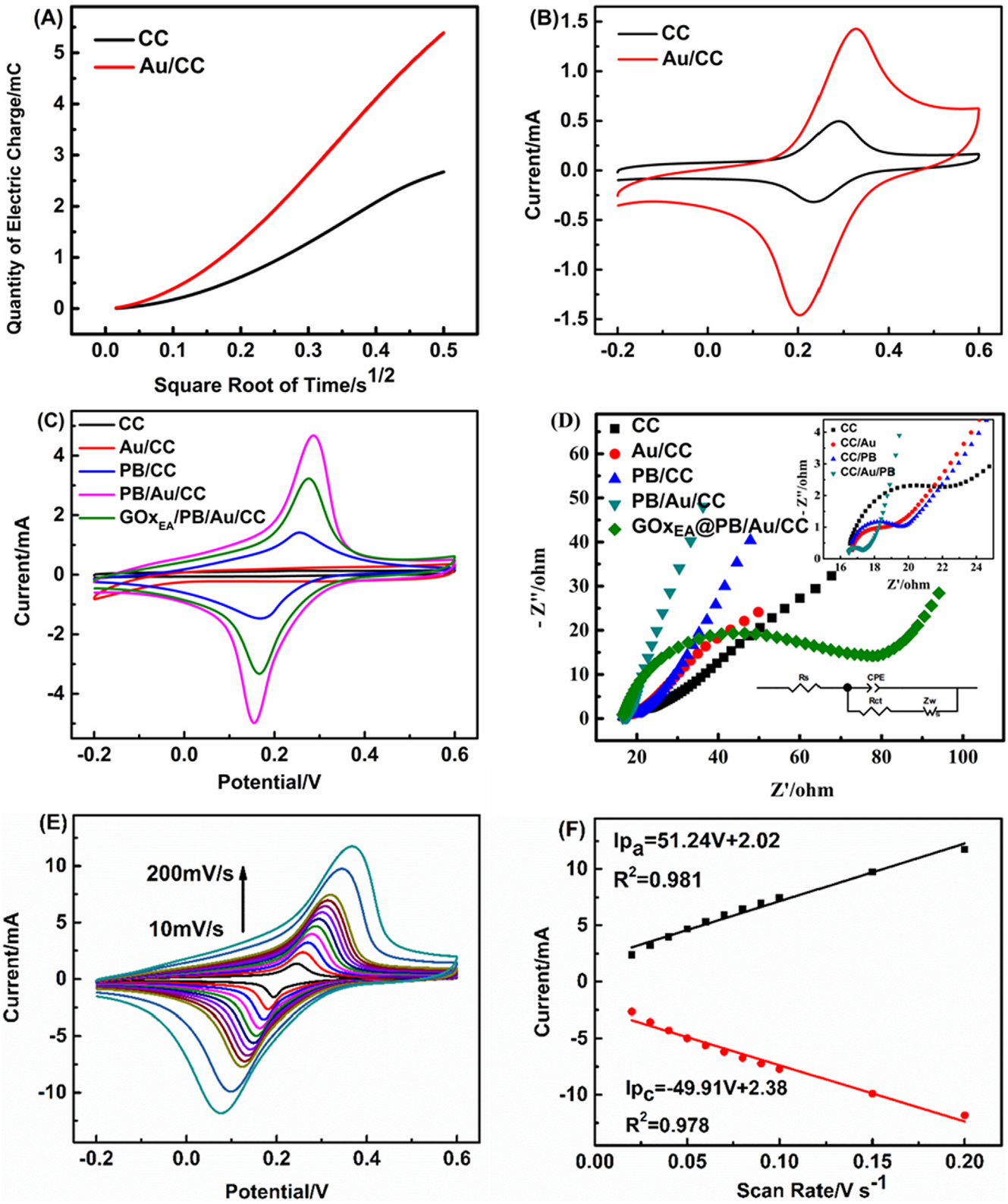

Fig. 2. (A) The chronocoulometric curves and (B) CVs of bare CC, Au/CC electrodes in 1 mM $[Fe(CN)_6]^{4-/3-}$ dissolved in 0.1 M KCl. (C) CVs and (D) EIS of bare CC, Au/CC, PB/CC, PB/Au/CC, GOx_{EA}@PB/Au/CC electrodes in 1 mM $[Fe(CN)_6]^{4-/3-}$ dissolved in 0.1 M KCl. The inset shows the corresponding equivalent circuit. (E) CVs of PB/Au/CC in different scan rates in 0.1 M PBS (pH 6.0) containing 0.1 M KCl. (F) The calibration plot of the peak current versus the scan rate.

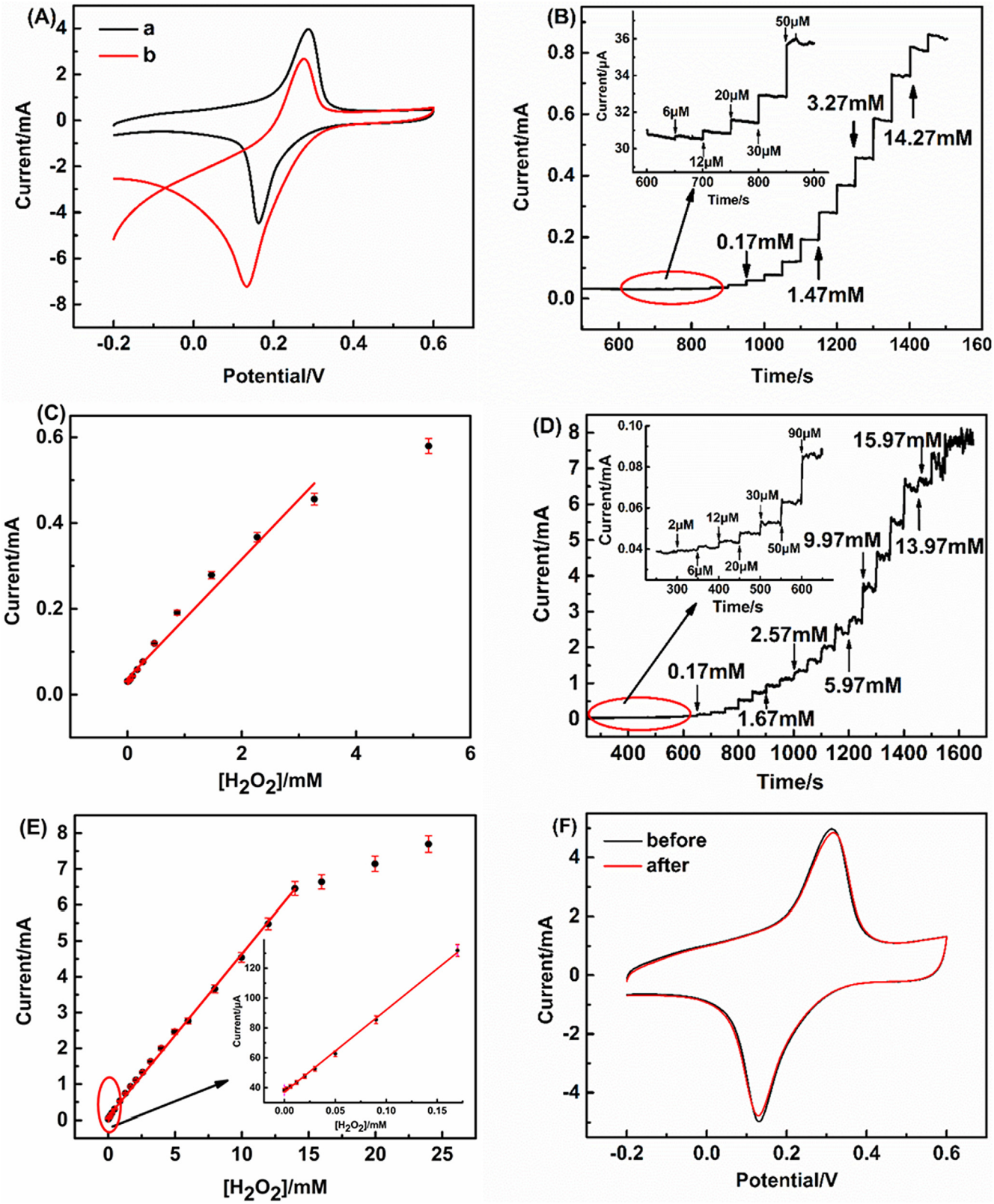

Fig. 3. (A) The CV responses of the PB modified Au/CC electrodes in 0.1 M PBS (pH 6.0) containing 0.1 M KCl in the (a) absence and (b) presence of 2 mM H_2O_2 at a scan rate of 50 mV s^{-1}. The amperometric responses of (B) PB/CC and (D) PB/Au/CC with the successive addition of H_2O_2 under the constant applied potential of −0.05 V. The calibration plot of the response current on (C) PB/CC and (E) PB/Au/CC versus H_2O_2 concentration. (F) CVs obtained at PB/Au/CC (a) before and (b) after 200 scanning cycles.

Table 1
A comparison of analytical performances of H_2O_2 biosensors.

Electrode	Sensitivity (μA mM^{-1} cm^{-2})	LOD (μM)	Linear range (μM)	Ref.
LDH-CMC/HRP	220.4	12.4	20–6000	[37]
PDDA/Au/HRP	280	/	0–2	[38]
PMPD–PB/GCE	138.4	0.6	5–1000	[39]
PB-rGO/GCE	196.6	1.9	20–200	[40]
PB/PPy/CMC	456.8	5.23	20–1100	[41]
PB/GO/GCE	408.7	0.12	5–1200	[42]
PB/NGF	386.0	2.4	4–1600	[21]
PB/CC	139.1	2	6–3270	This work
PB/Au/CC	454.97	0.5	2–13970	

HRP: Horseradish peroxidase, PDDA: polydimethyldiallylammonium, GCE: glassy carbon electrode, LDH: layered double hydroxides, CMC: carboxymethyl chitosan, PMPD: poly(m-phenylenediamine), RGO: reduced graphene, PPy: polypyrrole, NGF: nitrogen-doped graphite foam

200 cycles in the presence of 2 mM H_2O_2. Fig. 3D shows that the peak current does not change significantly after scanning for 200 cycles, indicating excellent electrochemical stability of the PB layer on Au/CC.

3.4. Glucose determination by GOx_{EA}@PB/Au/CC

Given the excellent performance of the PB/Au/CC for H_2O_2 detection and the fact that H_2O_2 is the by-product of glucose enzymolysis, we further used it as the substrate to develop an electrochemical glucose biosensor by employing the cross-linking enzyme aggregates method to immobilize GOx. To verify that the GOx_{EA}@PB/Au/CC cascade catalyzes the oxidation of glucose, CV was used to evaluate the possibility

In Fig. 4A shows the CVs of the GOx_{EA}@PB/Au/CC in 0.1 M PBS (pH 6.0) containing 0.1 M KCl without or with glucose. Compared with the CV response without glucose, the oxidation peak current decreases, and the reduction peak current increases. It is because that glucose is catalytically oxidized into gluconolactone and by-product H_2O_2 by GOx in the presence of dissolved oxygen, as shown in Eq. (4). Then the resulting H_2O_2 can be reduced by PW as described in Section 3.3. The result shows that the glucose biosensor we constructed is feasible and straightforward.

$$GOx(FAD) + Glucose \rightarrow GOx(FADH_2) + Glucolactone \quad (3)$$

$$GOx(FADH_2) + O_2 \rightarrow GOx(FAD) + H_2O_2 \quad (4)$$

To further evaluate the performance of the constructed biosensor, the amperometric i-t plot was employed at a constant applied potential of −0.05 V to measure the analytical performance. The result illustrated by Fig. 4B showing the amperometry results in a calibration plot of steady-state current vs. [Glucose] (Fig. 4C), revealing a sensitivity (slope) of 70.76 μA mM^{-1} cm^{-2} (R^2 = 0.999). This curve of steady-state current vs. [Glucose] is linear up to 3.15 mM, and the LOD is 10 μM (S/N = 3). At the same time, we followed the traditional cross-linking enzyme instead of aggregates to immobilize enzyme on the PB/Au/CC surface for glucose sensing (Fig. 4D). And the sensitivity of GOx@PB/Au/CC is 14.48 μA mM^{-1} cm^{-2} with LOD of 50 μM (S/N = 3). It displays the absolute advantages of the cross-linking enzyme aggregate method in the field of enzyme immobilization.

Table 2 exhibits a comparison of some analytical parameters obtained in this work with the data published in the literature. The results demonstrate that the comprehensive performance of the glucose biosensor we constructed is competitive with the previously reported electrochemical sensors. As enzymes are sensitive elements in the sensing system, the performance of biosensors is directly proportional to the density of electrically active enzymes immobilized on the electrode. Therefore, the improvement in the performance is mainly because the cross-linking enzyme aggregates method greatly increases the amount of enzyme loaded on the electrode.

To evaluate the anti-interferent property of the proposed glucose biosensor, the amperometric response with additions of glucose and interferents was measured under the applied potential of −0.05 V. In here, the interference effects of ascorbic acid (AA), uric acid (UA), and dopamine (DA) on the biosensor were investigated to test their effect on glucose determination (Fig. 4F). The biosensor shows an extremely significant response to 2 mM glucose and very negligible response to 0.1 mM AA, 0.1 mM UA and 0.1 mM DA. After the addition of the interferents, 1 mM glucose was added into the solution and the biosensor responses as in the case with no interferents. It can be concluded that the biosensor has proved to be of good selectivity to glucose, which can be explained by the high sensitivity at the low detection potential here.

3.5 . Reproducibility and stability of GOx_{EA}@PB/Au/CC electrode

Reproducibility is an important parameter for the assessment of the sensing platform. Herein, the reproducibility of the glucose biosensor was studied through intra-assay and inter-assay relative standard deviation (RSD). The intra-assay RSD of GOx_{EA}@PB/Au/CC was determined by measuring 3 mM glucose five times with one electrode, for which the obtained value was 2.9%. For the inter-assay, five electrodes were used to determine 3 mM glucose, and the obtained RSD was 4.1%.

Moreover, when studying the long-term stability of the biosensor, the GOx_{EA}@PB/Au/CC were stored at 4 °C when not in use. And the electrode retained 90% of the initial current response to 3 mM glucose after two weeks. These results indicate that the designed sensing platform possesses acceptable reproducibility and good stability in glucose determination.

3.6. Determination of glucose in the human serum

To evaluate the applicability of GOx_{EA}@PB/Au/CC to real samples, different concentrations of standard glucose were added into human serum diluted 10 times with PBS to determine the recovery. Table 3 exhibits that recoveries from different serum samples are in the range of 98% to 104%. High consistency between the detected glucose level and the real, and low RSD prove that the biosensor can effectively determine glucose in actual serum samples, and possess high reliability and practicality.

4. Conclusions

In this work, we developed a feasible electrochemical biosensor to determine glucose based on the Prussian blue - enzyme aggregates cascade catalytic system. The coral-like gold micro/nanostructures were formed onto carbon cloth electrodes followed by

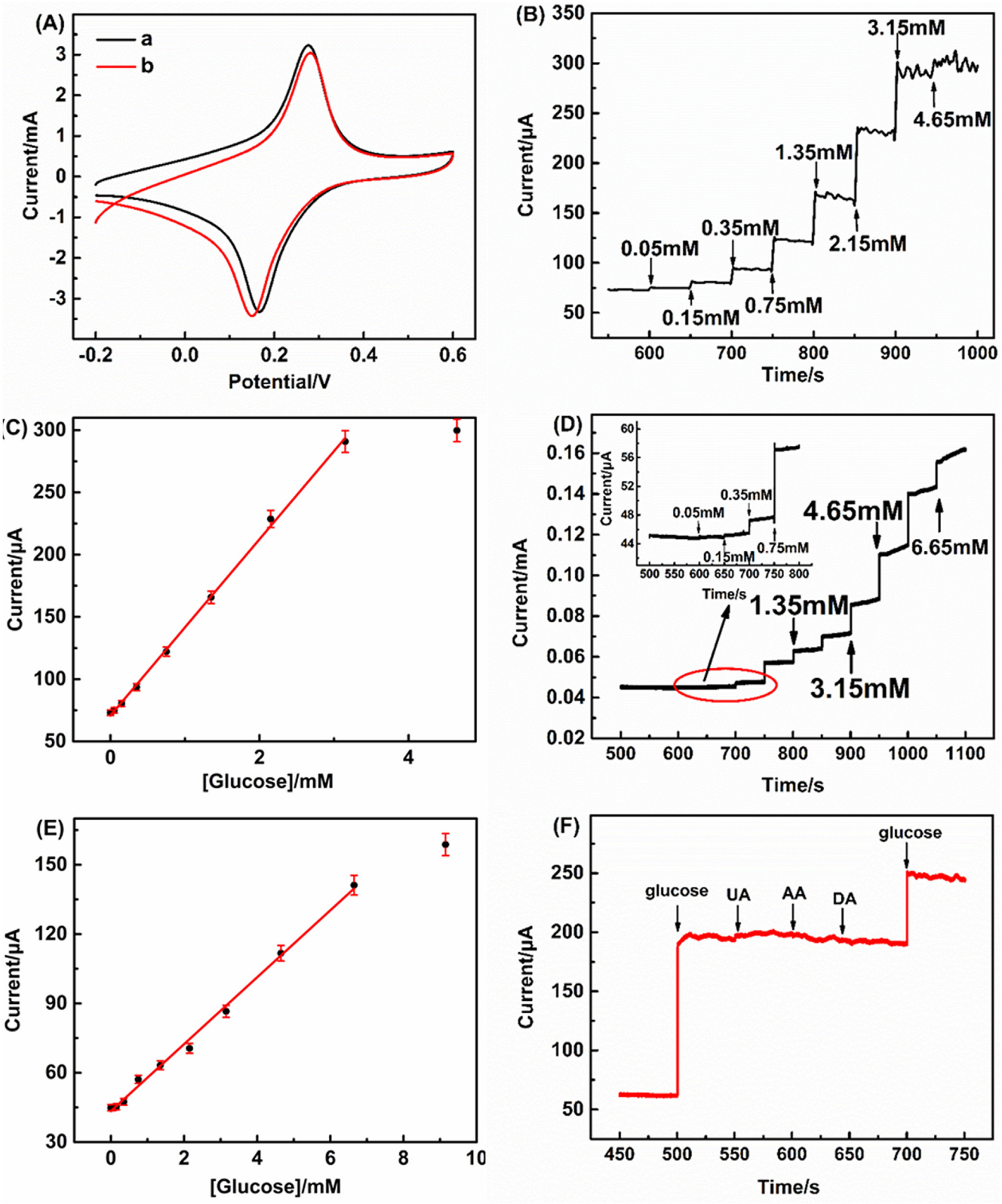

Fig. 4. (A) CVs of the GOx_{EA}@PB/Au/CC in 0.1 M PBS (pH 6.0) solution containing 0.1 M KCl: without (a) and with (b) glucose at a scan rate of 50 mV/s. (B) The amperometric curve obtained at the GOx_{EA}@PB/Au/CC in successive glucose addition. (C) The dependence of the response current on glucose concentration obtained at the GOx_{EA}@PB/Au/CC. (D) The amperometric curve obtained at the GOx@PB/Au/CC in successive glucose addition. (E) The dependence of the response current on glucose concentration obtained at the GOx@PB/Au/CC. (F) The amperometric curve of the GOx_{EA}@PB/Au/CC with the successive addition of 2 mM glucose, 0.1 mM UA, 0.1 mM AA, 0.1 mM DA and 1 mM glucose.

a Prussian blue electrochemical deposition process to construct a highly sensitive H_2O_2 biosensor. Due to the PB layer on the PB/Au/CC, the modified electrode possessed high electrochemical activity for H_2O_2 reduction. The PB/Au/CC electrode responded to H_2O_2 in the sensitivity of 454.97 μA mM^{-1} cm^{-2} within the linear range from 0.002 mM to 13.97 mM, with a detection limit of

Table 2
A comparison of analytical performances of glucose enzymatic biosensors.

Electrode	Referene electrode	E_{app} (V)	Sensitiviy ($\mu AmM^{-1}cm^{-2}$)	LOD (μM)	Linear range (mM)	Ref.
GOx/PB/PVP/MWCNT/Au	Ag/AgCl	−0.1	38	2	0.01–0.7	[43]
GOx/PB grid/Pt	Ag/AgCl	−0.1	34.8	200	0.02–1.5	[44]
GOx/Chit/IL/PB/Pt	Ag/AgCl	−0.05	37.8	5.0	0.01–4.2	[45]
GOx/PB/NGF	Ag/AgCl	−0.05	27.48	100	0.2–20	[21]
GOx/PB nancubes	Ag/AgCl	−0.05	83.4	10	0.01–1.3	[46]
GOx@PB/Au/CC	Ag/AgCl	−0.05	14.48	50	0.15–6.65	This work
GOx_{EA}@PB/Au/CC	Ag/AgCl	−0.05	70.76	10	0.05–3.15	

PVP: poly(4-vinylpyridine), MWCNTs: multiwalled carbon nanotubes, Chit: chitosan, IL: ionic liquid.

Table 3
Determination of glucose in real human serum samples using amperometry.

Sample	Added conc. (mM)	Found conc. (mM)	Recovery/%	RSD/%(n = 4)
Serum 1	0.50	0.52	104	4.3
Serum 2	1.00	1.01	101	3.7
Serum 3	1.50	1.47	98	3.3

0.5 μM (S/N = 3). And glucose biosensor was further constructed by immobilizing glucose oxidase using the cross-linking enzyme aggregates method onto the PB/Au/CC electrode surface. The present biosensor responded linearly to glucose in the concentration from 0.05 mM to 3.15 mM. Moreover, the sensitivity was 70.76 $\mu A\ mM^{-1}\ cm^{-2}$ and the detection limit was 10 μM (S/N = 3). The glucose biosensor exhibited a strong anti-interference ability to other electroactive materials such as ascorbic acid, uric acid, and dopamine. Furthermore, it also possessed good reproducibility and long-term stability, and the detection of glucose based on this sensor had high recovery in practical human serum samples. This biosensor is a reliable device and the proposed material and immobilization method could be used in several biosensor applications.

Declaration of Competing Interest

The authors declare that they have no known competing financial interests or personal relationships that could have appeared to influence the work reported in this paper.

Acknowledgements

This work was supported by the National Natural Science Foundation of China (No. 51772248) and the Seed Foundation of Innovation and Creation for Graduate Students at Northwestern Polytechnical University (No. CX2020212).

References

[1] J. Lee, K. Hyun, Y. Kwon, A study on the stability and sensitivity of mediator-based enzymatic glucose sensor measured by catalyst consisting of multilayer stacked via layer-by-layer, J. Ind. Eng. Chem. 93 (2021) 383–387.
[2] P. Raja, A.P. Maxwell, D.P. Brazil, The potential of albuminuria as a biomarker of diabetic complications, Cardiovasc. Drugs Ther. (2020).
[3] M. Adeel, M.M. Rahman, I. Caligiuri, V. Canzonieri, F. Rizzolio, S. Daniele, Recent advances of electrochemical and optical enzyme-free glucose sensors operating at physiological conditions, Biosens. Bioelectron. 165 (2020) 112331.
[4] J.P. Devadhasan, S. Kim, Toward CMOS image sensor based glucose monitoring, Analyst 137 (2012) 3917–3920.
[5] H. Ali, F. Bensaali, F. Jaber, Novel approach to non-invasive blood glucose monitoring based on transmittance and refraction of visible laser light, IEEE Access 5 (2017) 9163–9174.
[6] P. Virbickas, A. Valiūnienė, G. Kavaliauskaitė, A. Ramanavicius, Prussian white-based optical glucose biosensor, J. Electrochem. Soc. 166 (2019) B927–B932.
[7] L. Yan, P. Ma, Y. Liu, X. Ma, F. Chen, M. Li, 3D coral-like gold/carbon paper electrode modified with covalent and cross-linked enzyme aggregates for electrochemical sensing of glucose, Microchem. J. 159 (2020) 105347.
[8] H. Wang, Y. Ma, C. Guo, Y. Yang, Z. Peng, Z. Liu, et al., Templated seed-mediated derived Au nanoarchitectures embedded with nanochitosan: Sensitive electrochemical aptasensor for vascular endothelial growth factor and living MCF-7 cell detection, Appl. Surf. Sci. 481 (2019) 505–514.
[9] T. Bobrowski, W. Schuhmann, Long-term implantable glucose biosensors, Curr. Opin. Electrochem. 10 (2018) 112–119.
[10] C. Chen, X.-L. Zhao, Z.-H. Li, Z.-G. Zhu, S.-H. Qian, A.J. Flewitt, Current and emerging technology for continuous glucose monitoring, Sensors 17 (2017) 182.
[11] N. German, A. Ramanaviciene, A. Ramanavicius, Formation and electrochemical evaluation of polyaniline and polypyrrole nanocomposites based on glucose oxidase and gold nanostructures, Polymers 12 (2020) 3026.
[12] N. German, A. Popov, A. Ramanaviciene, A. Ramanavicius, Formation and electrochemical characterisation of enzyme-assisted formation of polypyrrole and polyaniline nanocomposites with embedded glucose oxidase and gold nanoparticles, J. Electrochem. Soc. 167 (2020) 165501.
[13] M. Sharifi, R. Pothu, R. Boddula, G.R. Bardajee, Trends of biofuel cells for smart biomedical devices, Int. J. Hydrogen Energy 46 (2021) 3220–3229.
[14] Y. Wang, L. Zhang, K. Cui, S. Ge, P. Zhao, J. Yu, Paper-supported self-powered system based on a glucose/O2 biofuel cell for visual MICRORNA-21 sensing, ACS Appl. Mater. Interfaces 11 (2019) 5114–5122.
[15] M. Christwardana, Y. Chung, Y. Kwon, Co-immobilization of glucose oxidase and catalase for enhancing the performance of a membraneless glucose biofuel cell operated under physiological conditions, Nanoscale 9 (2017) 1993–2002.
[16] D.V. Vokhmyanina, K.D. Andreeva, M.A. Komkova, E.E. Karyakina, A.A. Karyakin, 'Artificial peroxidase' nanozyme – enzyme based lactate biosensor, Talanta 208 (2020) 120393.
[17] K. Jindal, M. Tomar, V. Gupta, CuO thin film based uric acid biosensor with enhanced response characteristics, Biosens. Bioelectron. 38 (2012) 11–18.
[18] X. Zhang, G. Li, D. Wu, X. Li, N. Hu, J. Chen, et al., Recent progress in the design fabrication of metal-organic frameworks-based nanozymes and their applications to sensing and cancer therapy, Biosens. Bioelectron. 137 (2019) 178–198.
[19] A.A. Karyakin, E.E. Karyakina, L. Gorton, The electrocatalytic activity of Prussian blue in hydrogen peroxide reduction studied using a wall-jet electrode with continuous flow, J. Electroanal. Chem. 456 (1998) 97–104.
[20] M.A. Komkova, E.E. Karyakina, A.A. Karyakin, Catalytically synthesized prussian blue nanoparticles defeating natural enzyme peroxidase, J. Am. Chem. Soc. 140 (2018) 11302–11307.
[21] Y. Zhang, B. Huang, F. Yu, Q. Yuan, M. Gu, J. Ji, et al., 3D nitrogen-doped graphite foam@Prussian blue: an electrochemical sensing platform for highly sensitive determination of H2O2 and glucose, Microchim. Acta 185 (2018) 86.
[22] A.I. Rekertaitė, A. Valiūnienė, P. Virbickas, A. Ramanavicius, Physicochemical characteristics of polypyrrole/(glucose oxidase)/(prussian blue)-based biosensor modified with Ni- and Co-hexacyanoferrates, Electroanalysis 31 (2019) 50–57.
[23] R.A. Sheldon, Cross-linked enzyme aggregates (CLEA®s): stable and recyclable biocatalysts, Biochem. Soc. Trans. 35 (2007) 1583–1587.
[24] J.D. Cui, S.R. Jia, Optimization protocols and improved strategies of cross-linked enzyme aggregates technology: current development and future challenges, Crit. Rev. Biotechnol. 35 (2015) 15–28.
[25] B.C. Kim, X. Zhao, H.-K. Ahn, J.H. Kim, H.-J. Lee, K.W. Kim, et al., Highly stable enzyme precipitate coatings and their electrochemical applications, Biosens. Bioelectron. 26 (2011) 1980–1986.
[26] R. Schoevaart, M.W. Wolbers, M. Golubovic, M. Ottens, A.P.G. Kieboom, F. van Rantwijk, et al., Preparation, optimization, and structures of cross-linked enzyme aggregates (CLEAs), Biotechnol. Bioeng. 87 (2004) 754–762.
[27] J.-M. Wu, Q.-E. Zhao, Activation of carbon cloth and concurrent precipitation of titania nanowires for enhanced adsorption and photocatalysis performance, Appl. Surf. Sci. 527 (2020) 146779.

[28] D. Moscone, D. D'Ottavi, D. Compagnone, G. Palleschi, A. Amine, Construction and analytical characterization of prussian blue-based carbon paste electrodes and their assembly as oxidase enzyme sensors, Anal. Chem. 73 (2001) 2529–2535.
[29] G.-M. Yang, X. Chen, J. Li, Z. Guo, J.-H. Liu, X.-J. Huang, Bubble dynamic templated deposition of three-dimensional palladium nanostructure catalysts: approach to oxygen reduction using macro-, micro-, and nano-architectures on electrode surfaces, Electrochim. Acta 56 (2011) 6771–6778.
[30] A. Popov, B. Brasiunas, A. Damaskaite, I. Plikusiene, A. Ramanavicius, A. Ramanaviciene, Electrodeposited gold nanostructures for the enhancement of electrochromic properties of PANI–PEDOT film deposited on transparent electrode, Polymers 12 (2020) 2778.
[31] A. Gong, Y. Zhao, M. He, B. Liang, K. Li, High-performance desalination of three-dimensional nitrogen-doped carbon framework reinforced Prussian blue in capacitive deionization, Desalination 505 (2021) 114997.
[32] H.P. Boehm, Surface oxides on carbon and their analysis: a critical assessment, Carbon 40 (2002) 145–149.
[33] M.J. Piernas-Muñoz, E. Castillo-Martínez, V. Roddatis, M. Armand, T. Rojo, K1−xFe2+x/3(CN)6·yH2O, Prussian Blue as a displacement anode for lithium ion batteries, J. Power Sources 271 (2014) 489–496.
[34] S. Khumngern, R. Jirakunakorn, P. Thavarungkul, P. Kanatharana, A. Numnuam, A highly sensitive flow injection amperometric glucose biosensor using a gold nanoparticles/polytyramine/Prussian blue modified screen-printed carbon electrode, Bioelectrochemistry 138 (2021) 107718.
[35] M. Wu, Q. Zhang, Y. Fang, C. Deng, F. Zhou, Y. Zhang, et al., Polylysine-modified MXene nanosheets with highly loaded glucose oxidase as cascade nanoreactor for glucose decomposition and electrochemical sensing, J. Colloid Interface Sci. 586 (2021) 20–29.
[36] K.-J. Huang, L. Wang, H.-B. Wang, T. Gan, Y.-Y. Wu, J. Li, et al., Electrochemical biosensor based on silver nanoparticles–polydopamine–graphene nanocomposite for sensitive determination of adenine and guanine, Talanta 114 (2013) 43–48.
[37] J. Yuan, S. Xu, H.-Y. Zeng, X. Cao, A. Dan Pan, G.-F. Xiao, et al., Hydrogen peroxide biosensor based on chitosan/2D layered double hydroxide composite for the determination of H2O2, Bioelectrochemistry 123 (2018) 94–102.
[38] V. Mani, B.V. Chikkaveeraiah, V. Patel, J.S. Gutkind, J.F. Rusling, Ultrasensitive immunosensor for cancer biomarker proteins using gold nanoparticle film electrodes and multienzyme-particle amplification, ACS Nano 3 (2009) 585–594.
[39] J.-Z. Tao, G.-R. Xu, H.-L. Hao, F.-X. Yang, K.-S. Ahn, W.-Y. Lee, Poly(m-phenylenediamine)–Prussian blue hybrid film formed by one-step electrochemical deposition for glucose biosensor, J. Electroanal. Chem. 689 (2013) 96–102.
[40] E. Jin, X. Lu, L. Cui, D. Chao, C. Wang, Fabrication of graphene/prussian blue composite nanosheets and their electrocatalytic reduction of H2O2, Electrochim. Acta 55 (2010) 7230–7234.
[41] S. Uzunçar, N. Özdoğan, M. Ak, Amperometric detection of glucose and H2O2 using peroxide selective electrode based on carboxymethylcellulose/polypyrrole and Prussian Blue nanocomposite, Materials Today, Communications (2020) 101839.
[42] Y. Zhang, X. Sun, L. Zhu, H. Shen, N. Jia, Electrochemical sensing based on graphene oxide/Prussian blue hybrid film modified electrode, Electrochim. Acta 56 (2011) 1239–1245.
[43] J. Li, J.-D. Qiu, J.-J. Xu, H.-Y. Chen, X.-H. Xia, The synergistic effect of prussian-blue-grafted carbon nanotube/poly(4-vinylpyridine) composites for amperometric sensing, Adv. Funct. Mater. 17 (2007) 1574–1580.
[44] Z. Chu, L. Shi, Y. Zhang, W. Jin, S. Warren, D. Ward, et al., Single layer Prussian blue grid as a versatile enzyme trap for low-potential biosensors, J. Mater. Chem. 22 (2012) 14874–14879.
[45] Y. Zhang, Y. Liu, Z. Chu, L. Shi, W. Jin, Amperometric glucose biosensor based on direct assembly of Prussian blue film with ionic liquid-chitosan matrix assisted enzyme immobilization, Sens. Actuators, B 176 (2013) 978–984.
[46] D. Jiang, Z. Chu, J. Peng, W. Jin, Screen-printed biosensor chips with Prussian blue nanocubes for the detection of physiological analytes, Sens. Actuators, B 228 (2016) 679–687.